Electroweak Physics at ATLAS

Geraldine Conti[*][†]

Harvard University, Cambridge

E-mail: Geraldine.Conti@cern.ch

Various electroweak measurements have already been performed at the ATLAS experiment since the start of the Large Hadron Collider (LHC) at CERN. A review of the latest results in W/Z and diboson physics will be given here. The W/Z physics results include the measurement of the high-mass Drell-Yan di-lepton production cross section, the $Wb(b)$ production cross section and the study of the transverse momentum of Z/γ^*. The latest WW, WZ, ZZ, $W\gamma$ and $Z\gamma$ production cross sections will be summarized, including updated WW and ZZ results. In particular, the ZZ^* channel has been added. The ATLAS diboson results are also used to set limits on charged triple gauge couplings (WWZ, $WW\gamma$) and on neutral triple gauge couplings ($Z\gamma\gamma$, $ZZ\gamma$, ZZZ).

---

[*]Speaker.

[†]On behalf of the ATLAS Collaboration

1. Introduction

The ATLAS detector is a general purpose particle detector for the Large Hadron Collider (LHC) at CERN [1]. As of November 2012, various electroweak measurements have already been performed at the ATLAS experiment using the 7 TeV dataset recorded in 2011. First results using part of the 8 TeV dataset recorded so far in 2012 are also already available. The electroweak measurements allow for precision tests of the electroweak dynamics of the Standard Model (SM), but also challenge Next-to-Next-to-Leading-Order (NNLO) QCD predictions. Differences between measurements and SM predictions could prove evidence for New Physics (NP). Diboson processes are an important source of background to Higgs decays into vector boson pairs, such as $H \to WW$ and $H \to ZZ$, and also to other NP processes. It is therefore very important to perform precise measurements of their production cross sections. A review of the latest results in W/Z and diboson physics will be given here. Among those, the following results will be discussed:

- High-mass Drell-Yan production cross section using 5 fb^{-1} of 7 TeV data

- $Wb(b)$ production cross section using 5 fb^{-1} of 7 TeV data

- Angular correlations in Drell-Yan lepton pairs to probe Z/γ^* transverse momentum using 5 fb^{-1} of 7 TeV data

- Diboson (WW, WZ, ZZ, $W/Z\gamma$) total and fiducial cross sections, as well as limits on triple gauge couplings. Results for $W/Z\gamma$ use 1 fb^{-1} of 7 TeV data, results for WW, WZ and ZZ use 5 fb^{-1} of the 7 TeV data. A result for ZZ using 6 fb^{-1} of 8 TeV data is also discussed.

2. Results

The fiducial and total cross sections are defined as follows :

$$\sigma_{\text{fiducial}} = \frac{N_{\text{obs}} - N_{\text{bkg}}}{\mathscr{L} \times C_{VV}} \quad \text{with :} \quad C_{VV} = \frac{N_{\text{reco,analysis cuts}}}{N_{\text{gen,fiducial cuts}}} \tag{2.1}$$

$$\sigma_{\text{total}} = \sigma_{\text{fiducial}} \times \frac{1}{BR \times A_{VV}} \quad \text{with :} \quad A_{VV} = \frac{N_{\text{gen,fiducial cuts}}}{N_{\text{gen,total}}} \tag{2.2}$$

where N_{obs} is the number of observed events, N_{bkg} is the number of background events and $\mathscr{L}$ is the integrated luminosity. Fiducial cross sections have the advantage of reducing the theory uncertainty and allowing for easier comparison with theory prediction.

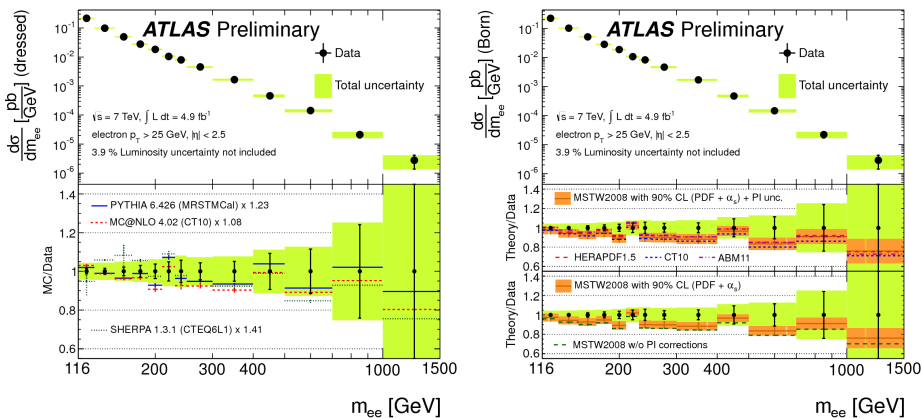### 2.1 Drell-Yan di-lepton production cross-section measurement

The Drell-Yan differential cross section is measured in the *ee* channel for di-electron masses between 116 GeV and 1500 GeV using 4.9 fb^{-1} of 7 TeV data [2]. Electrons are selected by requiring that their transverse energy is larger than 25 GeV and the absolute value of their pseudo-rapidity is smaller than 2.5. The di-electron mass spectrum is shown in Figure 1. A very good agreement between data and prediction is observed. The dominant backgrounds for this measurement are W+jets and di-jet contributions. They represent 6% to 16% of the sample, depending on the di-electron

mass. These backgrounds are estimated using data-driven techniques. The dominant uncertainties on the measurement come from the background estimates (1-8%), electron reconstruction and identification (3%) and electron energy scale and resolution (2-3%). The measurement is limited statistically for di-electron masses larger than about 500 GeV.
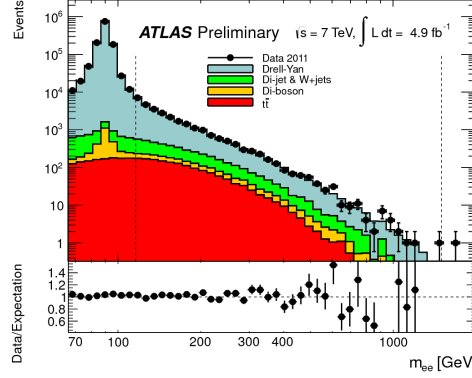
**Figure 1:** Di-electron mass spectrum [2].

The differential cross-section measurements as a function of the di-electron mass $m(ee)$ are shown in Figure 2, where the shape in data is compared with those predicted by different MC generators and by perturbative QCD at NNLO. The generators used are PYTHIA, MC@NLO and SHERPA. All of them show good agreement in shape with data. For the prediction of perturbative QCD at NNLO, the FEWZ 3.1 program is used with four sets of parton density funtions (PDF). Photon-induced corrections are added to the PDFs in the upper ratio plot in the figure on the right. The total uncertainty band arises from the PDF, α_s and photon-induced corrections. The lower ratio plot shows the influence of the photon-induced corrections on the MSTW2008 prediction. The uncertainty band only includes the PDF and α_s uncertainties. The agreement between data and prediction is improved when the photon-induced corrections are included.

Figure 2: Drell-Yan differential cross section as a function of $m(ee)$ in data compared to different generator predictions (left) and to perturbative QCD at NNLO (right) [2]. A good agreement with data is observed.

2.2 $Wb(b)$ production cross section measurement

The cross section for the production of a W boson in association with b-jets, $W(b)b$, has been measured separately for the 1-jet and 2-jet final states, and also for their combination, using 4.6 fb^{-1} of 7 TeV data [3]. In the 2-jet case, the combinations of $(b$-,b-$)$, $(b$-, c-$)$ and $(b$-,light-$)$ flavour jets are considered. The fiducial cross section is shown in Figure 3 for the electron and muon channels separately and their combination for the 1-jet, 2-jet and the combined final states. In the 1-jet final state, the measurements are consistent within 1.5 σ with the MCFM NLO predictions. In the 2-jet final state, a good agreement between data and prediction is observed. The combined fiducial cross section is $\sigma_{\text{fid}} = 7.1 \pm 0.5(\text{stat}) \pm 1.4(\text{syst})$ pb.
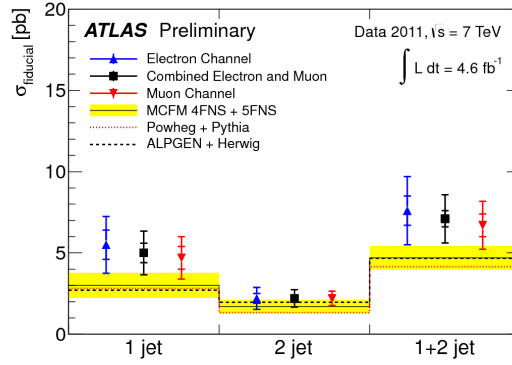
Figure 3: $Wb(b)$ fiducial cross section for the 1-jet and 2-jet final state, and their combination [3]. A good agreement between data and prediction is observed.
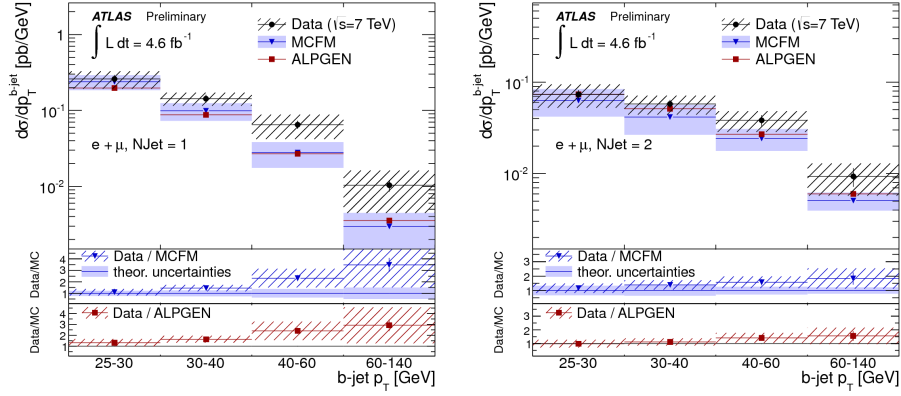
The differential cross section as a function of the leading b-jet p_{T} has also been calculated for jets with p_{T} ranging from 25 GeV to 140 GeV. Results are shown in Figure 4 for the 1-jet and 2-jet final states separately. In the former case, the measurement is larger than the predictions from MCFM (NLO) and Alpgen (LO), but compatible with a combination of the theory and experimental uncertainties. In the latter case, a good agreement is observed between data and prediction.

2.3 Angular correlations in Drell-Yan lepton pairs to probe Z/γ^* transverse momentum

A new variable to probe the $p_{\text{T}}(Z)$ domain, called ϕ_η^*, is suggested in [4]. It is defined as:

$$\phi_\eta^* = \tan(\phi_{\text{acop}}/2)\sin(\theta_\eta^*), \text{with} \quad \phi_{\text{acop}} = \pi - \Delta\phi \quad \text{and} \quad cos(\theta_\eta^*) = \tanh\left(\frac{\eta^- - \eta^+}{2}\right), \quad (2.3)$$

where $\Delta\phi$ is the azimuthal opening angle between the leptons and θ_η^* is the scattering angle of leptons with respect to the beam direction in the rest frame of the dilepton system. The ϕ_η^* variable is correlated with $p_{\text{T}}(Z)/m_{ll}$, hence probes the same physics as $p_{\text{T}}(Z)$, however with a better experimental resolution. The low p_{T}^Z spectrum dominates the Z/γ^* cross section. It is important to understand it precisely to further improve the modelling of W boson production in QCD calculation and MC event generators, as the W mass measurement is affected by p_{T}^W shape uncertainties. Moreover, the transverse-momentum resummation formalism required to describe the Z/γ^* boson cross section is also valid for the Higgs boson production.

Figure 4: Differential cross sections as a function of the leading *b*-jet p_T for the 1-jet (left) and 2-jet (right) final states [3]. A good agreement between data and prediction is observed for the latter case. For the former case, the measurement is compatible with prediction within a combiniation of the theory and experimental uncertainties.

Events with two same flavor leptons ($p_T^l > 20$ GeV and $|\eta^l| < 2.4$) are selected, which have an invariant mass of 66 GeV $< m_{ll} <$ 116 GeV. The dominant backgrounds are QCD multijet at low ϕ_η^*, $t\bar{t}$ and dibosons at high ϕ_η^*. The total experimental uncertainty achieved by the combination of electron and muon data is smaller than 0.5% for $\phi_\eta^* < 0.5$ and 0.8% for larger ϕ_η^* values.

Figure 5 shows the differential cross section as a function of ϕ^* using 4.7 fb^{-1} of 7 TeV data and is compared to NNLL calculations (RESBOS) [5]. These calculations are unable to reproduce the detailed shape of the measured cross section to better than 4%.
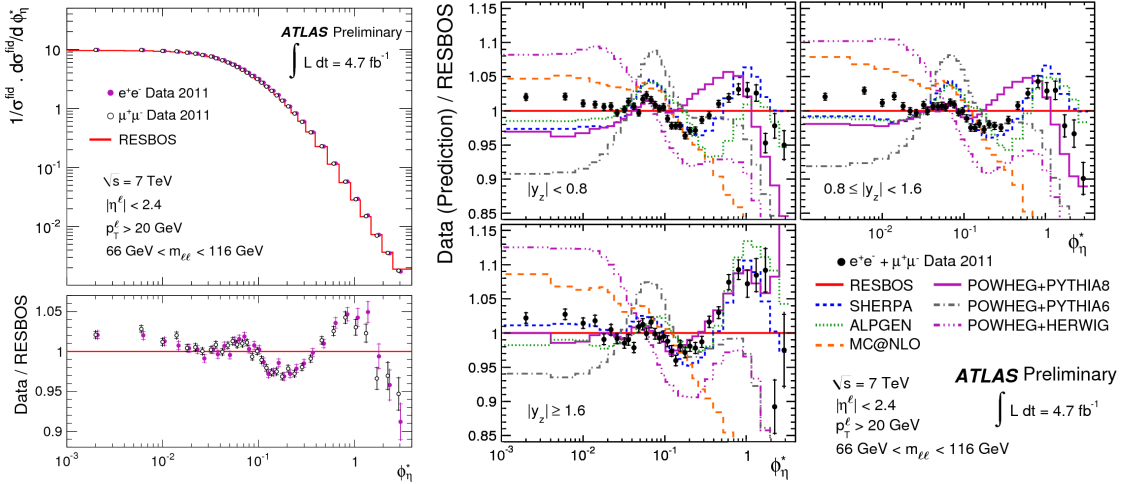
Figure 5: Differential cross section as a function of ϕ^* in data and comparison with NNLL calculation (RESBOS) (left) and ratio of the combined normalised differential cross sections to the RESBOS prediction as a function of ϕ_η^* for the three *Z* rapidity $|y_Z|$ ranges and comparison to predictions obtained using different MC event generators (right) [5].

The ratio of the combined normalised differential cross sections to the RESBOS prediction is shown in Figure 5 as a function of ϕ_η^* for three *Z* rapidity ranges : $|y_Z| < 0.8$, $0.8 < |y_Z| <$

1.6, $|y_Z| > 1.6$. The cross-section measurement is also compared to predictions from different Monte Carlo generators interfaced to a parton shower algorithm. Among these, SHERPA and POWHEG+PYTHIA8 Monte Carlo event generators give the best descriptions of the measured ϕ_η^*. For $\phi_\eta^* > 0.1$, SHERPA predictions are able to reproduce the data within $\sim 2\%$. The low ϕ_η^* spectrum is however more accurately described by RESBOS. The information provided by these double differential measurements as a function of ϕ_η^* and y_Z is valuable for the tuning of MC generators. Among the tested predictions, none is able to reproduce the detailed shape of the measured cross section within the experimental precision, which is about one order of magnitude smaller that the present theoretical uncertainties.

2.4 Diboson production cross sections and limits on anomalous Triple Gauge Couplings

A precise measurement of the diboson production cross sections is very important, as it is a very good test of the Standard Model. Discrepancies with respect to the SM could indicate presence of New Physics. Diboson is also a major irreducible background contribution to Higgs and NP scenarios. Both the total and fiducial cross sections are measured by the ATLAS experiment for the various diboson channels summarized in Table 1 [6]-[11]. Among those, the $WW \to l\nu l\nu$ [6], $ZZ(*) \to llll$ [11] and the $WW/Z \to l\nu qq$ [7] ones are new results firstly presented at the HCP conference held in Japan on 12-16 November 2012. Also, differential cross sections in bins of variables sensitive to new theories are provided. Triple Gauge Couplings (TGC), charged ones ($WW\gamma$, WWZ) and neutral ones ($Z\gamma\gamma$, $ZZ\gamma$, ZZZ), are also measured and act as a good probe for NP as well.

Diboson channel	WW	WZ	$W\gamma$	ZZ	$Z\gamma$
Decay channels	$l\nu l\nu$, $l\nu qq$	$l\nu ll$	$l\nu\gamma$	$llll$, $ll\nu\nu$	$ll\gamma$

**Table 1:** Diboson channels and their decay channels used in the measurements.

The production of diboson mainly happens via $q - \bar{q}$, at LO and NLO orders. At NLO order, the gluon-gluon fusion contributes too, however this counts for $\sim 3 - 6\%$ of the total production cross section. The production modes are depicted in Figure 6 for the WW, ZZ and WZ cases and in Figure 7 for the $W/Z\gamma$ case. At tree level, charged triple gauge couplings (WWZ, $WW\gamma$) are allowed in the SM, but not the neutral ones ($Z\gamma\gamma$, $ZZ\gamma$, ZZZ).

A first evidence (3.3σ) of diboson WW/Z production decaying into $l\nu qq$ channel is reported [7]. The $WW/Z \to l\nu qq$ channel has larger backgrounds than the fully leptonic WW/Z decays, but a larger branching ratio (43.8% compared to 4.7% for the $l\nu l\nu$ case with $l = e, \mu$). To select the events, the following selection criteria are applied: the presence of exactly two jets with $p_T(j_1) > 30$ GeV and $p_T(j_2) > 25$ GeV, $|\eta| < 2.5$, $\Delta R(j_1, j_2) > 0.7$ and $|\Delta\eta(j_1, j_2)| < 1.5$. In addition, a missing energy energy > 30 GeV is requested, as well as a transverse mass $m_T > 40$ GeV and a $\Delta\phi(\text{MET}, j_1) > 0.8$. The di-jet mass distribution after selection is shown in Figure 8 before and after background subtraction.

The measured total diboson production cross sections are summarized in Figure 9. They are generally slightly higher than the SM prediction, however consistent within uncertainties. The main uncertainty for the $W\gamma$ and $Z\gamma$ measurements come from photon identification (11% for $E_T > 15$ GeV, 4.5% for $E_T > 60$ GeV). The main uncertainty for the $WW \to l\nu l\nu$ and $ZZ \to ll\nu\nu$
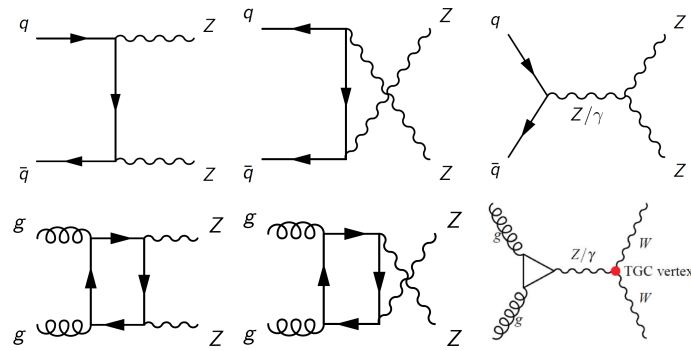
Figure 6: Example of ZZ production via $q - \bar{q}$ (top) and via gluon-gluon fusion (bottom), for t-channel (left), u-channel (middle) and s-channel (right) [10][11]. Similar production mechanisms apply for WW/Z.
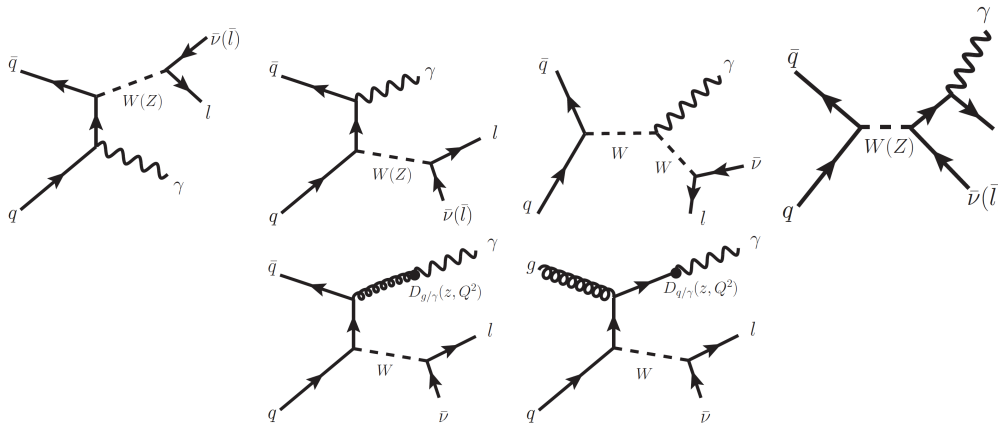

Figure 7: $W/Z\gamma$ production via $q - \bar{q}$ (top) for t-channel (left), u-channel (middle left), s-channel (middle right) and FSR (right) [9]. The photon can also emerge from the hard fragmentation of the final state parton (bottom): quark (left) or gluon (right).
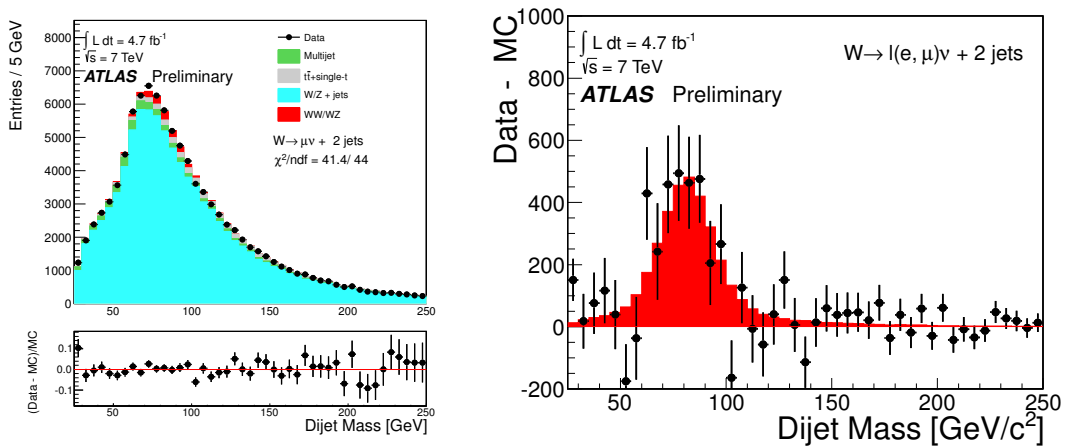

Figure 8: Di-jet mass distribution before (left) and after (right) background subtraction [7].

measurements is due to jet veto (3.6% and 5.3% respectively). In the case of $WW/Z \to l\nu qq$, the errors are dominated by the jet energy scale (12%) and the W/Z+jets normalization (11%). Finally, in the case of $WZ \to l\nu ll$ and $ZZ \to llll$, the errors are dominated by the electron identification efficiency (3.5% for *eee*, 2.3% for *eeμ*, 3.8% for *eeee*, 1.9% for *eeμμ*) and the muon reconstruction efficiency (0.8% for *μμμ*, 0.5% for *μμe*, 1.0% for *μμμμ*, 0.5% for *μμee*).
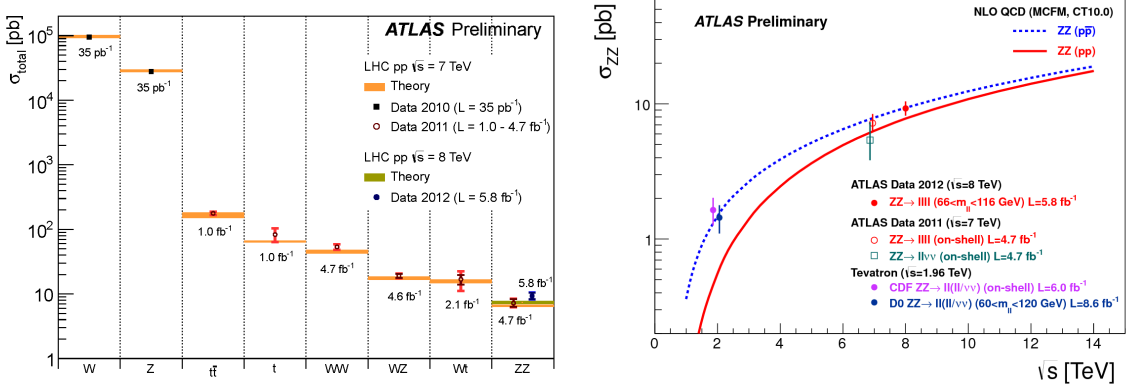
Figure 9: Summary of total diboson production cross-section measurements from the ATLAS experiment (left) [12] and summary for *ZZ* measurements including comparisons with measurements performed at Tevatron and with NLO predictions (right) [11].

Fiducial cross sections are also provided in bins of observables sensitive to new theories. For example, the p_T of the leading lepton is used in the case of $WW(l\nu l\nu)$ and $m(ZZ)$ is used in the $ZZ(llll)$ case. The corresponding fiducial cross sections are shown in Figure 10 as a function of those observables. Overall, all the measured fiducial cross sections are also found to be slightly higher than prediction, however within uncertainties.
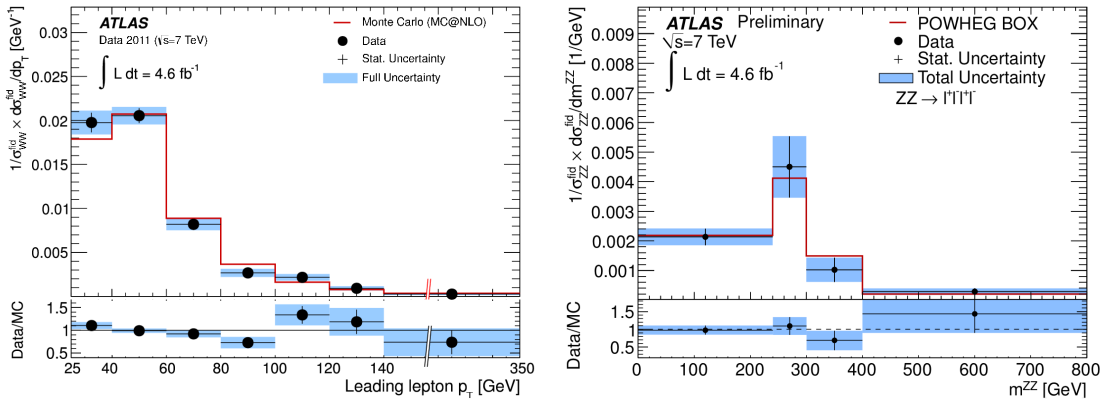
Figure 10: Fiducial cross sections as a function of leading lepton pT measured from $WW(l\nu l\nu)$ channel (left) [6] and as a function of $m(ZZ)$ from $ZZ(llll)$ channel (right) [10].

Triple Gauge Couplings are parameterized by CP-violating and CP-conserving complex parameters. Deviations from the SM values would increase the production cross sections and alter kinematic distributions (especially for large p_T). Limits at 95% CL are determined using different limit setting approaches : profile likelihood ratio in the *ZZ* case [10], frequentist limits in the *WZ*

case [8] or bayesian likelihood limits in the $WW/W/Z\gamma$ cases [6][9]. Systematic uncertainties are included as nuisance parameters in the fit. The triple-gauge coupling parameters that are tested in the following are summarized in Table 2.

WWZ	$WW\gamma$	$Z\gamma\gamma$	$ZZ\gamma$	ZZZ
$\Delta g_1^Z = g_1^Z - 1$	$\Delta\kappa_\gamma = \kappa_\gamma - 1$	$h_3^\gamma=0$	$h_3^Z=0$	$f_4^Z = 0$
$\Delta\kappa_Z = \kappa_Z - 1$	$\lambda_\gamma = 0$	$h_4^\gamma=0$	$h_4^Z=0$	$f_5^Z = 0$
$\lambda_Z = 0$			$f_4^\gamma=0$	
			$f_5^\gamma=0$	

Table 2: Triple-gauge coupling parameters to be tested and their SM prediction [6]-[11].

Figure 11 shows the triple-gauge coupling parameters measured for the charged vertices, WWZ ($\Delta g_1^Z = g_1^Z - 1$, $\Delta\kappa_Z = \kappa_Z - 1$, λ_Z) and $WW\gamma$ ($\Delta\kappa_\gamma = \kappa_\gamma - 1$, λ_γ [1]), using the WW (left), WZ (middle) and $W\gamma$ (right) channels. All the measurements are consistent with zero. The higher energies and higher diboson cross sections at the LHC have allowed for better constraints than the Tevatron results, and the approaching of the LEP combined limits.

Figure 12 shows the triple-gauge coupling parameters measured for the neutral vertices, $Z\gamma\gamma$ (h_3^γ, h_4^γ), $ZZ\gamma$ (h_3^Z, h_4^Z, f_4^γ, f_5^γ) and ZZZ (f_4^Z, f_5^Z) using the $Z\gamma$ (left, middle) and ZZ (right) channels. All the measurements are consistent with zero. More stringent limits have been obtained compared to Tevatron and LEP results.
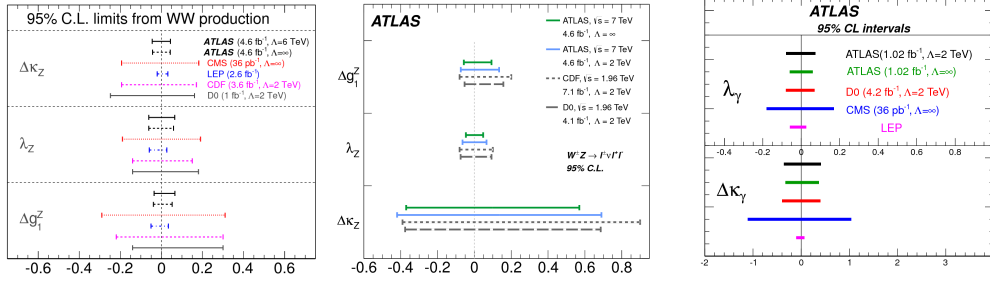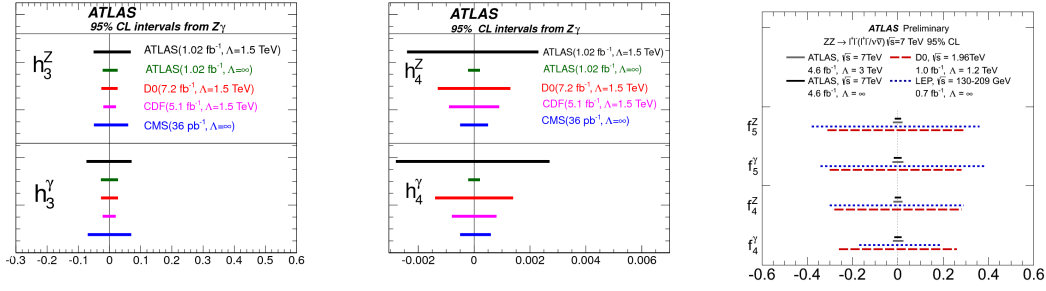

Figure 11: Triple-gauge coupling parameters measured for charged vertices using the WW (left) [6], WZ (middle) [8] and $W\gamma$ (right) channels [9].

3. Conclusions

A variety of electroweak measurements, which challenge the (NNLO) QCD predictions, has already been performed by the ATLAS collaboration. Among them here are reported the measurement of the high-nass Drell-Yan differential cross section, of the $W(b)b$ production cross section, the study of the transverse momentum of the Z/γ^* using the ϕ^* variable and the evidence of the $WZ+WW$ production in the $l\nu qq$ channel. All of the results show good agreement between data and SM expectation. The diboson cross sections measured are also in good agreement with SM expectation within uncertainties. The limits on possible non-SM anomalies resulting in anomalous triple gauge couplings have been tightened compared to the Tevatron and LEP results.

---

[1]For the WW measurement, the LEP scenario is applied, in which case $\lambda_Z = \lambda_\gamma$ and $\Delta\kappa_Z = \Delta\kappa_\gamma$.

Figure 12: Triple-gauge coupling parameters measured for neutral vertices using the $Z\gamma$ (left, middle) [9] and ZZ (right) channels [10].

References

[1] The ATLAS collaboration, *The ATLAS Experiment at the CERN Large Hadron Collider*, *JINST* **3** (2008) S08003.

[2] The ATLAS collaboration, *Measurement of the high-mass Drell-Yan differential cross-section in pp collisions at $\sqrt{s}$ =7 TeV with the ATLAS detector*, [ATLAS-CONF-2012-159].

[3] The ATLAS collaboration, *Measurement of the cross-section for W boson production in association with b-jets in pp collisions at $\sqrt{s}$ =7 TeV with the ATLAS detector*, [hep-ex/1320.2929]

[4] A. Banfi et al., *Optimisation of variables for studying dilepton transverse momentum distributions at hadron colliders*, *Eur. Phys. J.* **71** (2011) 1600 [hep-ex/1009.1580].

[5] The ATLAS collaboration, *Measurement of the angular correlations in Drell-Yan lepton pairs to probe Z/γ^* boson transverse momentum at $\sqrt{s}$ =7 TeV with the ATLAS detector*, *Phys. Lett. B.* **720** (2013) 32-51 [hep-ex/1211.6899].

[6] The ATLAS collaboration, *Measurement of W^+W^- production in pp collisions at $\sqrt{s}$ =7 TeV with the ATLAS detector and limits on anomalous WWZ and $WW\gamma$ couplings*, [hep-ex/1210.2979].

[7] The ATLAS collaboration, *Measurement of the combined WW and WZ production cross section in the semileptonic final state in proton-proton collisions at $\sqrt{s}$ =7 TeV with the ATLAS detector*, [ATLAS-CONF-2012-157]

[8] The ATLAS collaboration, *Measurement of $W^\pm Z$ production in Proton-Proton collisions at $\sqrt{s}$ =7 TeV with the ATLAS detector*, *Eur. Phys. J. C* **72** (2012) 2173 [hep-ex/1208.1390].

[9] The ATLAS collaboration, *Measurement of W gamma and Z gamma production cross section in pp collisions at $\sqrt{s}$ =7 TeV and limits on anomalous triple gauge couplings with the ATLAS detector*, *Phys. Lett. B* **717** (2012) 49 [hep-ex/12052531].

[10] The ATLAS collaboration, *Measurement of ZZ production in pp collisions at $\sqrt{s}$ =7 TeV and limits on anomalous ZZZ and ZZgamma couplings with the ATLAS detector*, [hep-ex/1211.6096]

[11] The ATLAS collaboration, *Measurement of the total ZZ production cross section in the four-lepton channel using 5.8 fb^{-1} of ATLAS data at $\sqrt{s}$ =8 TeV*, [ATLAS-CONF-2012-090].

[12] The ATLAS collaboration, *ATLAS Physics Summary Plots*, [https://twiki.cern.ch/twiki/bin/view/AtlasPublic/CombinedSummaryPlots]